Efficiency and Optimality of 2-period Limit Cycle Walking

Fumihiko Asano

School of Information Science, Japan Advanced Institute of Science and Technology,
1-1 Asahidai, Nomi, Ishikawa 923-1292, JAPAN, e-mail: fasano@jaist.ac.jp

Abstract

This paper investigates the efficiency of a 2-period gait from the kinetic energy view-point. First, we formulate a steady 2-period gait for a compass-like bipedal robot by using a simple recurrence formula for the kinetic energy of an asymmetric rimless wheel. Second, we theoretically show that, in the case that the mean value of the hip angle is constant, the generated 2-period steady gait is less efficient than a 1-period symmetric one in terms of kinetic energy. We also show that the symmetric gait is not always optimal from another viewpoint. We then extend the analysis to biped walking and investigate the validity of the derived method through numerical simulations of virtual passive dynamic walking.

keywords: Limit cycle walking, 2-period gait, kinetic energy, efficiency, rimless wheel

1 Introduction

Limit cycle walkers based on the robot's own passive dynamics are good examples of efficient bipedal locomotion. Since McGeer's passive dynamic walking (PDW) [1], many follow-on studies have been undertaken all over the world. One of the major interests is achieving efficient level dynamic walking with small actuators. The authors have proposed several methods for generating efficient bipedal gaits. Among them, virtual passive dynamic walking (VPDW) [2] and parametrically excited walking [3] are the major examples.

Studies on PDW as a nonlinear hybrid dynamical system have also been conducted. Nonlinear phenomena in PDW are very complicated, and their investigation has proceeded with difficulty for the last decade. The most interesting phenomenon that passive-dynamic walkers exhibit is the period-doubling bifurcation and chaotic behavior discovered by Goswami *et al.* They discovered a period-doubling bifurcation in a passive gait on a gentle slope and numerically showed that a compass-like biped robot exhibits period-doubling bifurcation by changing the walking system's parameters such as slope and leg-mass location [4]. After that, Garcia *et al.* showed that the simplest walking model and kneed model also exhibit period-doubling bifurcation [5][6][7]. Goswami *et al.* [8] and Sano *et al.* [9] investigated the bifurcation mechanism by using the eigenvalues of the Poincaré return map. Osuka

and Kirihara experimentally confirmed the phenomenon [10]. In addition, controlling chaos in dynamic gaits has been investigated. The OGY method [11] and delayed feedback control (DFC) [12] are the major approaches to controlling or stabilizing chaos. These have been used for stabilizing a multiple period gait into a 1-period one. Sugimoto and Osuka used DFC to stabilize a passive-dynamic gait and generated an unstable 1-period gait [13]. Suzuki and Furuta also used the OGY method for the stabilization [14].

As manifested by the above studies, the period-doubling bifurcation phenomenon and the properties of multiple-period gaits in PDW have been widely studied. However, the reason why this phenomenon emerges has not yet been discovered, and the effects that bifurcation might have on gait efficiency are still unclear. Although the application of multiple-period or chaotic behavior to legged locomotion control has been expected, no useful methods have been proposed to date. It is known that the hip-joint damper can eliminate the chaotic behavior and create a 1-period limit cycle. This extends the stable domain and does not have any advantages from an engineering standpoint. Meanwhile, the authors observed that the efficiency of a 2-period gait grows worse rapidly after the first bifurcation point [15] and have shown that the gait efficiency of an asymmetric gait would be low.

Based on the observations, in this paper we investigate the efficiency and optimality of a 2-period gait in terms of the kinetic energy. The convergent kinetic energy is to be an indicator of gait efficiency. A steady 2-period gait is formulated by using recurrence formulas of kinetic energy just before impact of an asymmetric rimless wheel on the walking surface. This formula can specify the steady discrete dynamics of general 2-period limit cycle walking. We then theoretically investigate the relation between the gait efficiency and gait symmetry from a kinetic energy view-point, and mathematically derive the optimal condition under several assumptions. The validity of the derived methods is also investigated in a planar bipedal walking driven in accordance with the method of VPDW.

This paper is organized as follows. In Section II, we summarize the stability mechanism of a rimless wheel. In Section III, we formulate a steady 2-period gait based on two recurrence formulas of kinetic energy just before impact. In Section IV, the validity of the analysis is investigated through numerical simulations of VPDW. Finally, Section V concludes this paper and describes future research directions.

2 Stability Principle of a Rimless Wheel

We first describe the stability mechanism of a rimless wheel. Since the detailed theory was already explained in [18], we only outline it here.

Fig. 1 shows the model of a rimless wheel. Let α [rad] be the angle between the frames, and θ [rad] be the angle with respect to vertical. We assume that the total mass, M [kg], is concentrated at the central point and the leg frames have no mass. We also assume that $0 \leq \alpha \leq \pi$.

Let K^- [J] be the kinetic energy just before impact; it satisfies the following recurrence formula:

$$K^-[i+1] = \varepsilon K^-[i] + \Delta E, \tag{1}$$

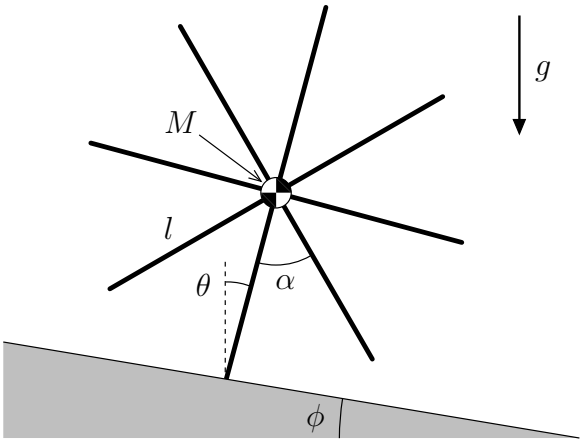

Figure 1: Rimless wheel model

where i is the step number, ε [-] is the energy-loss coefficient, and ΔE [J] is the restored mechanical energy. The energy-loss coefficient is defined as

$$\varepsilon := \frac{K^+}{K^-}, \tag{2}$$

where K^+ [J] is the kinetic energy just after impact. In this rimless wheel model, ε and ΔE are given by the following equations.

$$\varepsilon = \cos^2 \alpha \tag{3}$$

$$\Delta E = 2Mlg \sin \frac{\alpha}{2} \sin \phi \tag{4}$$

The generated gait becomes asymptotically stable under the assumption that the next heel-strike always occurs, and K^- converges to

$$K^-[\infty] := \lim_{i \to \infty} K^-[i] = \frac{\Delta E}{1 - \varepsilon}. \tag{5}$$

Note that ε is convex upward in the range of $0 \leq \alpha \leq \pi/4$, and ΔE is proportional to the step length. These properties are common to the original PDW [1] and VPDW [2], and they are very important for understanding the gait efficiency.

Since the 2-D rimless wheel model is a very simple way to reproduce the discrete walking behavior, it has often been used for analyzing gait efficiency and robustness [16][17]. In the following, we utilize it for representing the discrete dynamics of 2-period limit cycle walking.

3 Efficiency of an Asymmetric Rimless Wheel

3.1 Preliminaries

Fig. 2 shows the model of an asymmetric rimless wheel. Let α_1 and α_2 [rad] be the relative angles between the frames. We assume the following magnitude relation:

$$\alpha_2 \leq \alpha \leq \alpha_1, \tag{6}$$

where we also define their mean value, α [rad], as

$$\alpha := \frac{\alpha_1 + \alpha_2}{2}. \tag{7}$$

Let ε_j be the energy-loss coefficient and ΔE_j be the restored mechanical energy corresponding to the angle α_j, as follows.

$$\varepsilon_j := \varepsilon(\alpha_j) = \cos^2 \alpha_j \quad (j = 1, 2) \tag{8}$$

$$\Delta E_1 = 2Mlg \sin \frac{\alpha}{2} \sin \left(\phi + \frac{\alpha_1 - \alpha_2}{4} \right) \tag{9}$$

$$\Delta E_2 = 2Mlg \sin \frac{\alpha}{2} \sin \left(\phi - \frac{\alpha_1 - \alpha_2}{4} \right) \tag{10}$$

Here, ΔE_i were derived from the law of conservation of mechanical energy, and are given as changes in potential energy. They satisfy the following magnitude relations.

$$\varepsilon_1 \leq \varepsilon \leq \varepsilon_2, \quad \Delta E_2 \leq \Delta E \leq \Delta E_1 \tag{11}$$

Since ε_j is convex upward in the range of $0 \leq \alpha_j \leq \pi/4$, the following magnitude relation holds:

$$\varepsilon \geq \frac{\varepsilon_1 + \varepsilon_2}{2} \geq \sqrt{\varepsilon_1 \varepsilon_2}, \tag{12}$$

where the second inequality is an arithmetic and geometric means inequality. The equalities in Eq. (12) hold when $\alpha_1 = \alpha_2$. On the other hand, the mean value of restored mechanical energy can be written as follows:

$$\frac{\Delta E_1 + \Delta E_2}{2} = 2Mlg \sin \frac{\alpha}{2} \sin \phi \cos \frac{\alpha_1 - \alpha_2}{4}. \tag{13}$$

This leads to the following magnitude relation:

$$\Delta E \geq \frac{\Delta E_1 + \Delta E_2}{2}. \tag{14}$$

The equality holds when $\alpha_1 = \alpha_2$.

By using the above variables, we can formulate the discrete dynamics of a rimless wheel. Let K_j^- be the kinetic energy just before an impact corresponding to the hip angle, α_j. The following two recurrence formulas hold.

$$K_2^-[2i+1] = \varepsilon_1 K_1^-[2i] + \Delta E_2 \tag{15}$$

$$K_1^-[2i+2] = \varepsilon_2 K_2^-[2i+1] + \Delta E_1 \tag{16}$$

In the following, we will analyze the gait efficiency of an asymmetric rimless wheel in terms of kinetic energy.

3.2 Optimality when α is constant

We first investigate the case in which α [rad] is constant. By substituting Eq. (15) into Eq. (16) and eliminating K_2^-, we obtain

$$K_1^-[2i+2] = \varepsilon_1 \varepsilon_2 K_1^-[2i] + \varepsilon_2 \Delta E_2 + \Delta E_1. \tag{17}$$

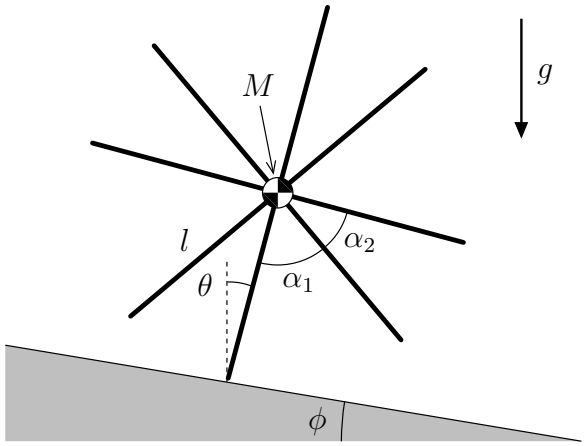

Figure 2: Asymmetric rimless wheel model

This leads to

$$K_1^-[\infty] = \frac{\varepsilon_2 \Delta E_2 + \Delta E_1}{1 - \varepsilon_1 \varepsilon_2}. \tag{18}$$

In the same way, we obtain

$$K_2^-[\infty] = \frac{\varepsilon_1 \Delta E_1 + \Delta E_2}{1 - \varepsilon_1 \varepsilon_2}. \tag{19}$$

The mean value becomes

$$K_m^-[\infty] := \frac{1}{2}\left(K_1^-[\infty] + K_2^-[\infty]\right) = \frac{\varepsilon_1 \Delta E_1 + \varepsilon_2 \Delta E_2 + \Delta E_1 + \Delta E_2}{2(1 - \varepsilon_1 \varepsilon_2)}. \tag{20}$$

Define the mean values of Eqs. (12) and (14) as

$$\varepsilon_m := \frac{\varepsilon_1 + \varepsilon_2}{2}, \tag{21}$$

$$\Delta E_m := \frac{\Delta E_1 + \Delta E_2}{2}, \tag{22}$$

and consider the following magnitude relation:

$$\varepsilon_m \Delta E_m - \frac{\varepsilon_1 \Delta E_1 + \varepsilon_2 \Delta E_2}{2} = \frac{(\varepsilon_2 - \varepsilon_1)(\Delta E_1 - \Delta E_2)}{4} \geq 0$$

and the relation of arithmetic and geometric means of Eq. (12),

$$\varepsilon_m \geq \sqrt{\varepsilon_1 \varepsilon_2}. \tag{23}$$

The upper limit of Eq. (20) can then be derived as

$$K_m^-[\infty] \leq \frac{\varepsilon_m \Delta E_m + \Delta E_m}{1 - \varepsilon_m^2} = \frac{(1 + \varepsilon_m)\Delta E_m}{(1 + \varepsilon_m)(1 - \varepsilon_m)} = \frac{\Delta E_m}{1 - \varepsilon_m}. \tag{24}$$

This is the upper limit of $K_m^-[\infty]$ common to general 2-period gaits.

By using the two magnitude relations of Eqs. (12) and (14), the magnitude relation for $K^-[\infty]$ can be derived as follows.

$$K_m^-[\infty] \leq \frac{\Delta E_m}{1 - \varepsilon_m} \leq \frac{\Delta E}{1 - \varepsilon} = K^-[\infty] \tag{25}$$

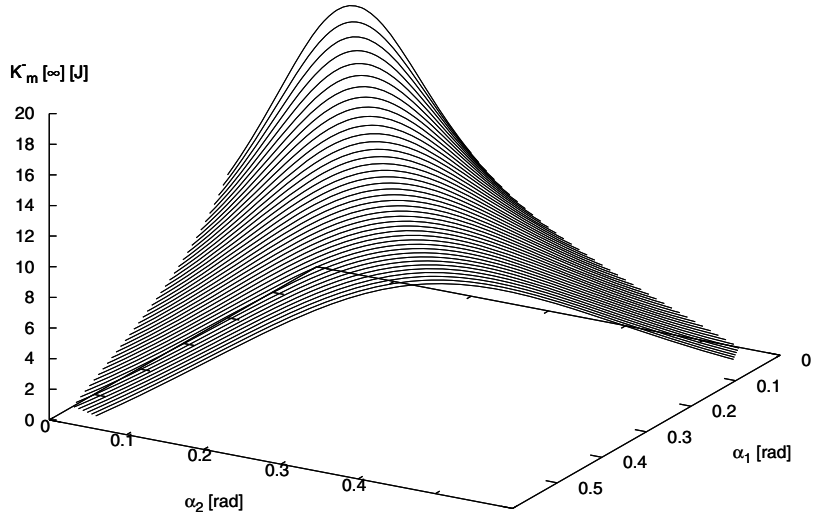

Figure 3: 3D plot of $K_m^-[\infty]$ with respect to α_1 and α_2

The equality holds when $\Delta E = \Delta E_m$ and $\varepsilon = \varepsilon_m$, and this is equivalent to $\alpha_1 = \alpha_2 = \alpha$.

Fig. 3 shows the 3D plot of $K_m^-[\infty]$ with respect to α_1 and α_2 where $M = 20.0$ [kg] and $l = 1.0$ [m]. The 3D plot was drawn with convex curves. Each curve corresponds to a given constant α ($0.10 \leq \alpha \leq 0.30$). We can see that the optimal solution is $\alpha_1 = \alpha_2 (= \alpha)$ on each curve.

As $\alpha_1 \to 2\alpha$ and $\alpha_2 \to 0$, the generated gait becomes a symmetric 1-period gait whose recurrence formula is

$$K_1^-[i+1] = \varepsilon_1 K_1^-[i] + \Delta E_1, \tag{26}$$

where $\varepsilon_1 = \cos^2(2\alpha)$ and $\Delta E_1 = 2Mlg \sin\alpha \sin\phi$. In this case, the convergent kinetic energy becomes the lowest.

Based on the above discussion, we can conclude that gait efficiency grows worse as the gait changes into a 2-period one because the step grows larger or the energy-loss coefficient becomes smaller.

The magnitude relation (Eq. (14)) holds for a dynamic bipedal gait such as PDW [1] or VPDW [2]. The relation for the energy-loss coefficient, however, does not always hold because it is affected by the angular velocities just before impact. Except for the gait with a constraint on the impact posture [18], the condition of Eq. (12) cannot be guaranteed.

3.3 Optimality when α_1 is constant

Fig. 4 plots the contour of the 3D plot in Fig. 3 in the α_1-α_2 plane. We can see that the contour is symmetric with $\alpha_1 = \alpha_2$. Note that the optimal solution, $\alpha_1 = \alpha_2$, is obtained in the case that the mean value, α, is constant (See direction A in Fig. 4).

In the case that α_1 is fixed, the optimal solution does not become $\alpha_1 = \alpha_2$, as one can see from direction B in Fig. 4.

Let α_1 be constant. Partially differentiating Eq. (20) with respect to α_2 yields

$$\frac{\partial K_m^-[\infty]}{\partial \alpha_2} = \frac{Mlg\sin\phi}{2\left(1-\cos^2\alpha_1\cos^2\alpha_2\right)^2}F(\alpha_2), \tag{27}$$

where

$$F(\alpha_2) = \cos\frac{\alpha_2}{2}\left(1+\cos^2\alpha_2\right)\left(1-\cos^2\alpha_1\cos^4\alpha_2\right) - 2\sin(2\alpha_1)\left(1+\cos^2\alpha_1\right)\left(\sin\frac{\alpha_1}{2}\cos^2\alpha_1 + \sin\frac{\alpha_2}{2}\right). \tag{28}$$

It is not easy to find the solution of α_2 for $F(\alpha_2) = 0$ analytically. Fig. 5 plots $K_m^-[\infty]$ with respect to α_2 for five values of α_1. We can see that the optimal solutions are not at $\alpha_1 = \alpha_2$ in all cases.

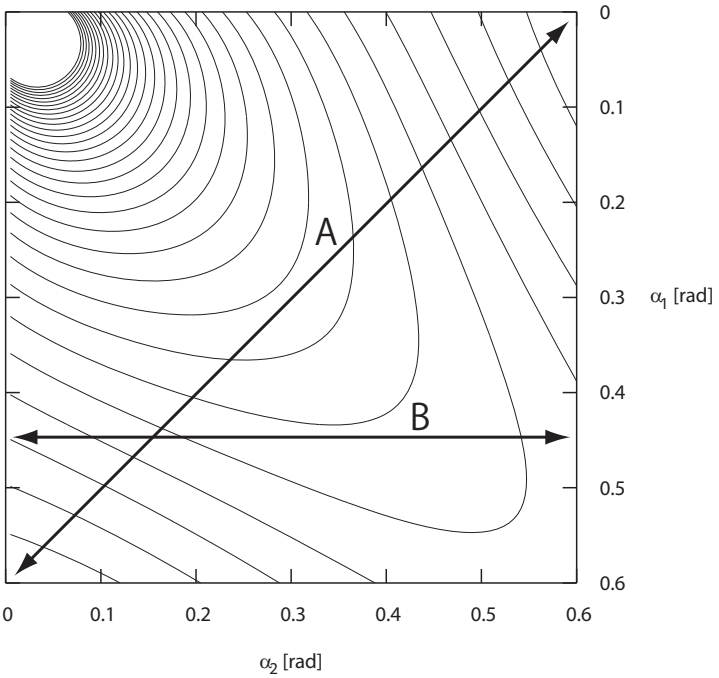

Figure 4: Contour of $K_m^-[\infty]$ with respect to α_1 and α_2

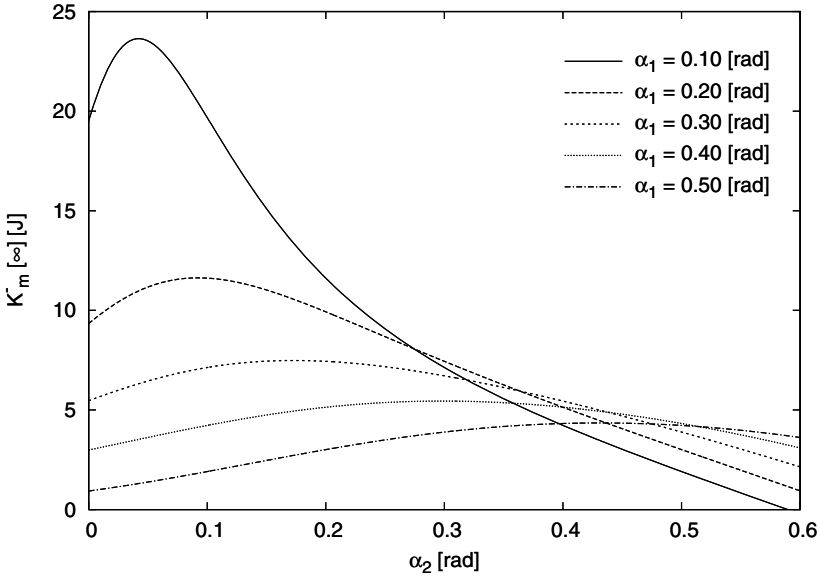

Figure 5: α_2 versus $K_m^-[\infty]$ for five values of α_1

4 Virtual Passive Dynamic Walking

This section investigates the validity of the analysis in the previous section through numerical simulations of VPDW.

4.1 Biped robot model

Fig. 6 shows a planar fully actuated biped model. Since the model is the same as those of [2][18], we only outline it. This model consists of 2-link and 3-point masses and has feet whose mass and thickness can be neglected. Let $\boldsymbol{\theta} = \left[\begin{array}{cc} \theta_1 & \theta_2 \end{array} \right]^{\mathrm{T}}$ be the generalized coordinate vector; the robot's dynamic equation is

$$\boldsymbol{M}(\boldsymbol{\theta})\ddot{\boldsymbol{\theta}} + \boldsymbol{h}(\boldsymbol{\theta}, \dot{\boldsymbol{\theta}}) = \boldsymbol{S}\boldsymbol{u} = \left[\begin{array}{cc} 1 & 1 \\ 0 & -1 \end{array} \right] \left[\begin{array}{c} u_1 \\ u_2 \end{array} \right], \tag{29}$$

where u_1 and u_2 are the ankle and hip joint torques. The matrices are described in detail elsewhere. If we assume inelastic collisions for the stance-leg exchange and set suitable values for the physical parameters, the robot can exhibit passive dynamic walking on a gentle slope. Let E be the total mechanical energy of the robot, and relationship $\dot{E} = \dot{\boldsymbol{\theta}}^{\mathrm{T}} \boldsymbol{S}\boldsymbol{u}$ between the mechanical energy and the control inputs holds.

The modeling of an inelastic collision is briefly described here. A more detailed explanation is given elsewhere. We extended the configuration as shown in Fig. 7. We define the stance and swing legs just before impact as "Leg 1" and "Leg 2" and derive their dynamic models independently. We define $\boldsymbol{q}_i = \left[\begin{array}{ccc} x_i & z_i & \theta_i \end{array} \right]^{\mathrm{T}}$ as the extended coordinate vector for Leg i and define $\boldsymbol{q} = \left[\begin{array}{cc} \boldsymbol{q}_1^{\mathrm{T}} & \boldsymbol{q}_2^{\mathrm{T}} \end{array} \right]^{\mathrm{T}}$ as that of the whole system. The inelastic collision model is then derived as

$$\bar{\boldsymbol{M}}(\boldsymbol{q})\dot{\boldsymbol{q}}^{+} = \bar{\boldsymbol{M}}(\boldsymbol{q})\dot{\boldsymbol{q}}^{-} - \boldsymbol{J}_I(\boldsymbol{q})^{\mathrm{T}}\boldsymbol{\lambda}_I, \tag{30}$$

where $\bar{\boldsymbol{M}}(\boldsymbol{q}) \in \mathbb{R}^{6\times 6}$ is the inertia matrix corresponding to $\boldsymbol{q}$, and superscripts "+" and "−" respectively stand for just after and just before impact. The $\boldsymbol{J}_I(\boldsymbol{q}) \in \mathbb{R}^{4\times 6}$ is the Jacobian matrix derived from the geometric constraint conditions at the instant of heel strike; it should satisfy the following velocity constraint condition just after impact:

$$\boldsymbol{J}_I(\boldsymbol{q})\dot{\boldsymbol{q}}^{+} = \boldsymbol{0}_{4\times 1}. \tag{31}$$

$\boldsymbol{\lambda}_I \in \mathbb{R}^4$ is Lagrange's undetermined multiplier vector within the context of impulsive force, and can be derived following Eqs. (30) and (31) as

$$\boldsymbol{\lambda}_I = \boldsymbol{X}_I(\boldsymbol{q})^{-1}\boldsymbol{J}_I(\boldsymbol{q})\dot{\boldsymbol{q}}^{-}, \quad \boldsymbol{X}_I(\boldsymbol{q}) := \boldsymbol{J}_I(\boldsymbol{q})\boldsymbol{M}(\boldsymbol{q})^{-1}\boldsymbol{J}_I(\boldsymbol{q})^{\mathrm{T}} \tag{32}$$

In the following, we describe the derivation of $\boldsymbol{J}_I(\boldsymbol{q})$. The velocity constraint conditions between the two legs to connect them are derived from geometric conditions such that the Leg 1's hip is positioned the same as the Leg 2's, and they can be expressed as

$$\frac{\mathrm{d}}{\mathrm{d}t}\left(x_1 + l\sin\theta_1\right)^{+} = \frac{\mathrm{d}}{\mathrm{d}t}\left(x_2 + l\sin\theta_2\right)^{+}, \tag{33}$$

$$\frac{\mathrm{d}}{\mathrm{d}t}\left(z_1 + l\cos\theta_1\right)^{+} = \frac{\mathrm{d}}{\mathrm{d}t}\left(z_2 + l\cos\theta_2\right)^{+}. \tag{34}$$

These are arranged as

$$\dot{x}_1^+ + l\dot{\theta}_1^+ \cos\theta_1 = \dot{x}_2^+ + l\dot{\theta}_2^+ \cos\theta_2, \tag{35}$$

$$\dot{z}_1^+ - l\dot{\theta}_1^+ \sin\theta_1 = \dot{z}_2^+ - l\dot{\theta}_2^+ \sin\theta_2. \tag{36}$$

Further, the contact condition with the ground of the post-impact stance-foot is given by

$$\dot{x}_2^+ = 0, \quad \dot{z}_2^+ = 0. \tag{37}$$

Summarizing the above four conditions of Eqs. (35), (36) and (37), $\boldsymbol{J}_I(\boldsymbol{q})$ yields

$$\boldsymbol{J}_I(\boldsymbol{q}) = \begin{bmatrix} 1 & 0 & l\cos\theta_1 & -1 & 0 & -l\cos\theta_2 \\ 0 & 1 & -l\sin\theta_1 & 0 & -1 & l\sin\theta_2 \\ 0 & 0 & 0 & 1 & 0 & 0 \\ 0 & 0 & 0 & 0 & 1 & 0 \end{bmatrix}. \tag{38}$$

Here, define the half inter-leg angle at impact

$$\alpha := \frac{\theta_1^- - \theta_2^-}{2} = \frac{\theta_2^+ - \theta_1^+}{2} > 0, \tag{39}$$

then we can find that the matrices $\bar{\boldsymbol{M}}$, $\boldsymbol{J}_I$ and $\boldsymbol{X}_I$ are functions only of α because all of them are related only to the angular positions θ_i. For example, $\theta_1(=\theta_1^-)$ and $\theta_2(=\theta_2^-)$ in Eq. (38) are equal to α and $-\alpha$. In the following, we will describe the functions only of angular positions as those of α.

Following Eqs. (30) and (31), we can derive the velocity vector just after impact as

$$\dot{\boldsymbol{q}}^+ = \left(\boldsymbol{I}_6 - \bar{\boldsymbol{M}}(\alpha)^{-1}\boldsymbol{J}_I(\alpha)^{\mathrm{T}}\boldsymbol{X}_I(\alpha)^{-1}\boldsymbol{J}_I(\alpha)\right)\dot{\boldsymbol{q}}^- =: \boldsymbol{Y}(\alpha)\dot{\boldsymbol{q}}^-. \tag{40}$$

The relation between $\dot{\boldsymbol{q}}^-$ and $\dot{\boldsymbol{\theta}}^-$ is given by

$$\dot{\boldsymbol{q}}^- = \begin{bmatrix} 0 & 0 \\ 0 & 0 \\ 1 & 0 \\ l\cos\theta_1 & -l\cos\theta_2 \\ -l\sin\theta_1 & l\sin\theta_2 \\ 0 & 1 \end{bmatrix} \begin{bmatrix} \dot{\theta}_1^- \\ \dot{\theta}_2^- \end{bmatrix} =: \boldsymbol{H}(\alpha)\dot{\boldsymbol{\theta}}^-. \tag{41}$$

In addition, by achieving the constraint on impact posture, the angular velocity just before impact can be written as

$$\dot{\boldsymbol{\theta}}^- = \begin{bmatrix} 1 \\ 1 \end{bmatrix} \dot{\theta}_1^-. \tag{42}$$

Summarizing Eqs. (40), (41) and (42), the angular velocity vector just after impact is given by

$$\dot{\boldsymbol{\theta}}^+ = \begin{bmatrix} 0 & 0 & 0 & 0 & 0 & 1 \\ 0 & 0 & 1 & 0 & 0 & 0 \end{bmatrix} \boldsymbol{Y}(\alpha)\boldsymbol{H}(\alpha) \begin{bmatrix} 1 \\ 1 \end{bmatrix} \dot{\theta}_1^- =: \boldsymbol{\xi}(\alpha)\dot{\theta}_1^-. \tag{43}$$

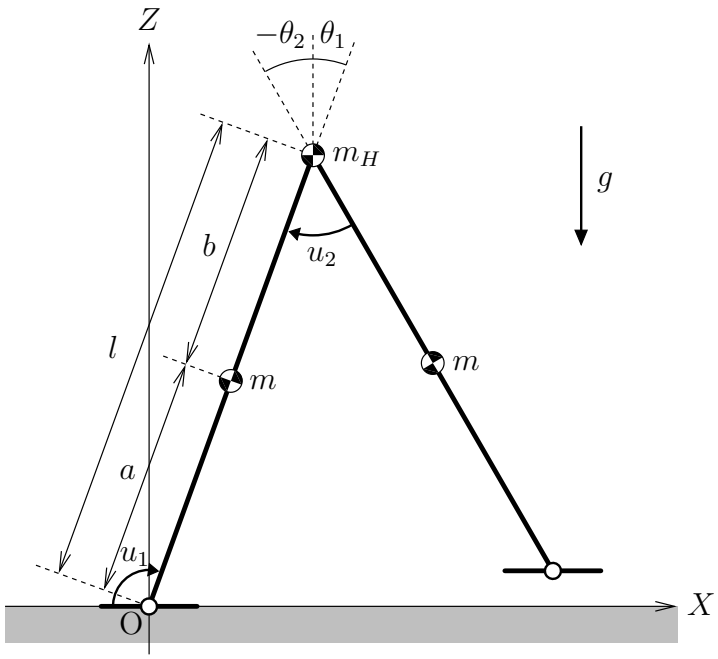

Figure 6: Model of planar fully actuated compass-like biped robot

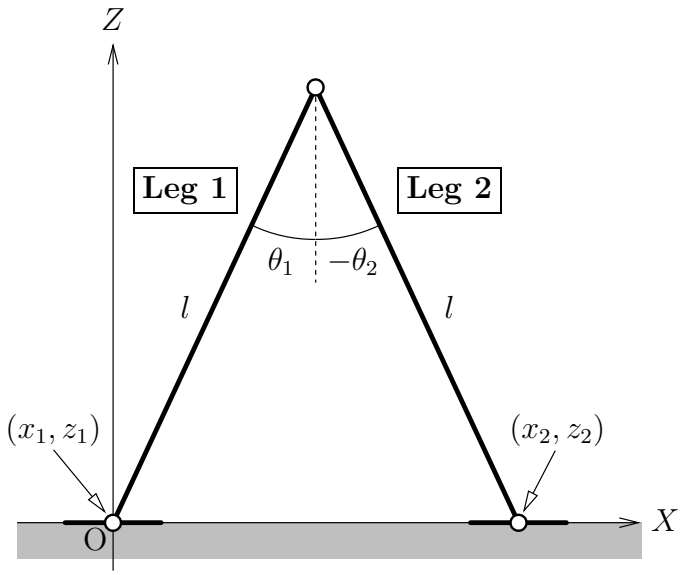

Figure 7: Configuration at instant of heel strike

4.2 Controller synthesis and typical 2-period gait

As the most basic approach to achieve the two magnitude relations of Eq. (12) and (14), we can consider VPDW with a constraint on the impact posture, which is termed as the constrained compass-gait. In our previous work [18], we applied high-gain PD feedback to the hip-joint control ignoring the effect of ankle-joint torque. In this approach, however, negligible but small tracking error remains. This paper then considers more accurate control approach.

In VPDW, the joint torques are determined to satisfy the following relation between the X-position of CoM, X_g, and the total mechanical energy:

$$\frac{\partial E}{\partial X_g} = Mg\tan\phi, \tag{44}$$

where ϕ [rad] is the virtual slope angle and $M := m_H + 2m$ [kg] is the robot's total mass. Taking $\dot{E} = \dot{\boldsymbol{\theta}}^{\mathrm{T}}\boldsymbol{S}\boldsymbol{u}$ into account, we can expand Eq. (44) to

$$\dot{E} = \dot{\theta}_1 u_1 + \dot{\theta}_H u_2 = Mg\tan\phi\dot{X}_g, \tag{45}$$

and we determine u_1 and u_2 according to the priority order. Hence, we will realize VPDW with a constraint on the impact posture.

Next, we synthesize the motion controller for generating ΔE_2 in Eq. (15). During the stance phase, the hip angle θ_H must move smoothly during the change from $-2\alpha_1$ to $2\alpha_2$. We introduce the following 5-order desired-time trajectory.

$$\theta_{H\mathrm{d}}(t) = \begin{cases} a_{51}t^5 + a_{41}t^4 + a_{31}t^3 + a_{01} & (0 \le t < T_{\mathrm{set}}) \\ 2\alpha_2 & (t \ge T_{\mathrm{set}}) \end{cases} \tag{46}$$

The coefficients, a_{i1}, are determined so that they satisfy

$$\ddot{\theta}_{H\mathrm{d}}(0) = 0,\ \dot{\theta}_{H\mathrm{d}}(0) = 0,\ \theta_{H\mathrm{d}}(0) = -2\alpha_1,\ \ddot{\theta}_{H\mathrm{d}}(T_{\mathrm{set}}) = 0,\ \dot{\theta}_{H\mathrm{d}}(T_{\mathrm{set}}) = 0,\ \theta_{H\mathrm{d}}(T_{\mathrm{set}}) = 2\alpha_2, \tag{47}$$

and are given by

$$a_{51} = \frac{12(\alpha_1+\alpha_2)}{T_{\mathrm{set}}^5},\quad a_{41} = -\frac{30(\alpha_1+\alpha_2)}{T_{\mathrm{set}}^4},\quad a_{31} = \frac{20(\alpha_1+\alpha_2)}{T_{\mathrm{set}}^3},\quad a_{01} = -2\alpha_1. \tag{48}$$

The coefficients, a_{i2}, of the desired-time trajectory for generating ΔE_1 in Eq. (16) are determined in the same manner. a_{52}, a_{42}, and a_{32} are determined with the same equation as above and $a_{02} = -2\alpha_2$. The desired settling time, T_{set} [s], is chosen empirically. Let T_1 and T_2 [s] be the steady step periods; we found that a constrained compass-gait could be successfully generated if the settling-time condition, $T_{\mathrm{set}} \le T_1$ and T_2, is satisfied.

We then consider the output following control for the desired-time trajectory. We resolve the control input vector as

$$\boldsymbol{S}\boldsymbol{u} = \begin{bmatrix} 1 \\ 0 \end{bmatrix} u_1 + \begin{bmatrix} 1 \\ -1 \end{bmatrix} u_2 =: \boldsymbol{S}_1 u_1 + \boldsymbol{S}_2 u_2, \tag{49}$$

and conduct input-output linearization. The hip-joint angle for the control output can be written as $\theta_H = \boldsymbol{S}_2^{\mathrm{T}}\boldsymbol{\theta}$, and its second-order derivative with respect to time becomes

$$\ddot{\theta}_H = \boldsymbol{S}_2^{\mathrm{T}}\ddot{\boldsymbol{\theta}} = \boldsymbol{S}_2^{\mathrm{T}}\boldsymbol{M}(\boldsymbol{\theta})^{-1}\left(\boldsymbol{S}_1 u_1 + \boldsymbol{S}_2 u_2 - \boldsymbol{h}(\boldsymbol{\theta}, \dot{\boldsymbol{\theta}})\right). \tag{50}$$

Then we can consider the following condition for the tracking control:

$$\ddot{\theta}_H = v := \ddot{\theta}_{H\mathrm{d}} + k_{\mathrm{d}}\left(\dot{\theta}_{H\mathrm{d}} - \dot{\theta}_H\right) + k_{\mathrm{p}}\left(\theta_{H\mathrm{d}} - \theta_H\right), \tag{51}$$

where $k_{\rm p}$ and $k_{\rm d}$ are the PD gains and are positive constants. By summarizing the relations of Eqs. (45), (50) and (51), we can specify the condition for the control inputs as

$$\boldsymbol{\Phi}\boldsymbol{u} = \boldsymbol{\Gamma}, \tag{52}$$

where

$$\boldsymbol{\Phi} = \begin{bmatrix} \dot{\theta}_1 & \dot{\theta}_H \\ \boldsymbol{S}_2^{\rm T}\boldsymbol{M}(\boldsymbol{\theta})^{-1}\boldsymbol{S}_1 & \boldsymbol{S}_2^{\rm T}\boldsymbol{M}(\boldsymbol{\theta})^{-1}\boldsymbol{S}_2 \end{bmatrix}, \quad \boldsymbol{\Gamma} = \begin{bmatrix} Mg\tan\phi\dot{X}_g \\ v + \boldsymbol{S}_2^{\rm T}\boldsymbol{M}(\boldsymbol{\theta})^{-1}\boldsymbol{h}(\boldsymbol{\theta},\dot{\boldsymbol{\theta}}) \end{bmatrix}. \tag{53}$$

The control input is then determined as $\boldsymbol{u} = \boldsymbol{\Phi}^{-1}\boldsymbol{\Gamma}$. The problem is the regularity of matrix $\boldsymbol{\Phi}$, but it did not matter in the numerical simulations of this paper.

Fig. 8 shows the phase portrait of a steady 2-period constrained compass-gait where $\alpha_1 = 0.24$, $\alpha_2 = 0.16$, $T_{\rm set} = 0.75$ [s], and $\phi = 0.02$ [rad]. The physical parameters of the robot are chosen as listed in Table 1. The PD gains were chosen sufficiently large ($k_{\rm d} = 100$ and $k_{\rm p} = 2500$) to achieve trajectory tracking control and a constraint on the impact posture with satisfactory accuracy. The figure shows that we return to the original position after two laps.

Table 1: Physical parameters of biped robot

m_H	10.0	kg
m	5.0	kg
a	0.5	m
b	0.5	m
$l\ (=a+b)$	1.0	m

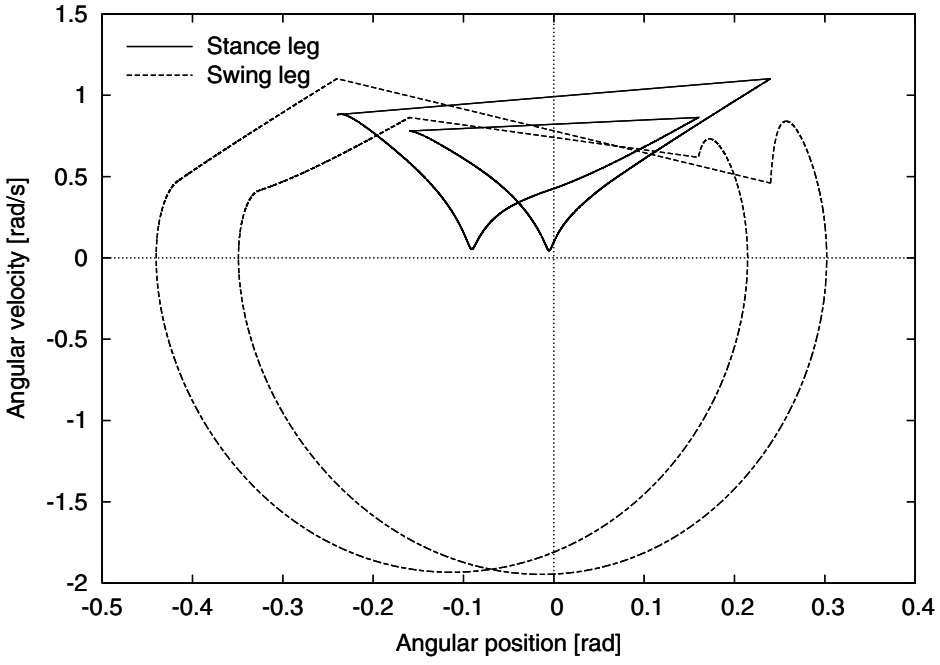

Figure 8: Phase portrait of steady 2-period constrained compass-gait

4.3 Restored mechanical energy

In 2-period gaits, the restored mechanical energy is determined not only by the control inputs but also by the difference in the potential energies at impact. Eq. (15) can be detailed as

$$K_2^-[\infty] + P_2[\infty] = \varepsilon_1 K_1^-[\infty] + P_1[\infty] + \int_{0^+}^{T_2^-} \dot{\boldsymbol{\theta}}^{\mathrm{T}} \boldsymbol{S}\boldsymbol{u} \, \mathrm{d}t, \tag{54}$$

where P_1 and P_2 are the potential energies corresponding to each impact. By grouping the terms in Eq. (54) except those of the kinetic energy, ΔE_2 of (15) can be derived as

$$\begin{aligned} \Delta E_2 &= \int_{0^+}^{T_2^-} \dot{\boldsymbol{\theta}}^{\mathrm{T}} \boldsymbol{S}\boldsymbol{u} \, \mathrm{d}t + P_1[\infty] - P_2[\infty] \\ &= Mgl \tan\phi \left(\sin\alpha_1 + \sin\alpha_2\right) + \left(m_H l + 2ma\right) g \left(\cos\alpha_1 - \cos\alpha_2\right). \end{aligned} \tag{55}$$

In the same way, ΔE_1 of Eq. (16) can be derived as

$$\Delta E_1 = Mgl \tan\phi \left(\sin\alpha_1 + \sin\alpha_2\right) - \left(m_H l + 2ma\right) g \left(\cos\alpha_1 - \cos\alpha_2\right). \tag{56}$$

From Eq. (46) and (47), the magnitude relation of Eq. (14) can be written as follows.

$$\Delta E_m = \frac{\Delta E_1 + \Delta E_2}{2} = 2Mgl \tan\phi \sin\alpha \cos\frac{\alpha_1 - \alpha_2}{2} \leq 2Mgl \tan\phi \sin\alpha = \Delta E \tag{57}$$

4.4 Energy-loss coefficient

Let $\theta_H^* > 0$ be the desired relative hip-angle at impact. If the impact posture is constrained and $\theta_H^- = \theta_H^*$, the energy-loss coefficient becomes

$$\varepsilon(\beta, \gamma, \theta_H^*) = \frac{N_\varepsilon(\beta, \gamma, \theta_H^*)}{D_\varepsilon(\beta, \gamma, \theta_H^*)}, \tag{58}$$

$$\begin{aligned} N_\varepsilon(\beta, \gamma, \theta_H^*) &= 4\beta^2\left(\beta(\beta-1)+1\right) + 2\beta\gamma(\beta+1) + \gamma^2 + 4\beta(\beta-1)(\beta+\gamma)\cos\theta_H^* \\ &\quad + \gamma(2\beta+\gamma)\cos(2\theta_H^*), \end{aligned} \tag{59}$$

$$D_\varepsilon(\beta, \gamma, \theta_H^*) = \left(2 + 2\beta(\beta-1) + \gamma + 2(\beta-1)\cos\theta_H^*\right)\left(1 + 2\beta^2 + 2\gamma - \cos(2\theta_H^*)\right), \tag{60}$$

where $\beta = a/l$ [-] and $\gamma = m_H/m$ [-]. The value for the simplest walking model [6] can be derived as

$$\lim_{\gamma\to\infty} \varepsilon(\beta, \gamma, \theta_H^*) = \cos^2\theta_H^*. \tag{61}$$

That is, ε is uniquely determined by the hip angles regardless of the leg-mass position. In addition, ε becomes 0 when $\theta_H^* = \pi/2$. In other words, the robot completely loses its kinetic energy and the motion stops if falling down with $\theta_H^* = \pi/2$.

Fig. 9 plots ε with respect to θ_H^* in the range of $0 \leq \theta_H^* \leq \pi$ for four values of γ where $\beta = 0.5$. Each ε has an absolute minimum in the neighborhood of $\theta_H^* = \pi/2$. Note that $\varepsilon = 0$ occurs only in the case of $\gamma = \infty$. In other words, existence of the leg mass enables the robot to avoid completely energy loss when the heel strikes the walking surface.

In general, θ_H^* is less than or comparable to about 0.30 [rad] in VPDW, and ε is convex upward in this range of values. The robot that we are considering here has $\gamma = 2.0$, and Fig. 9 clearly indicates that ε is convex upward.

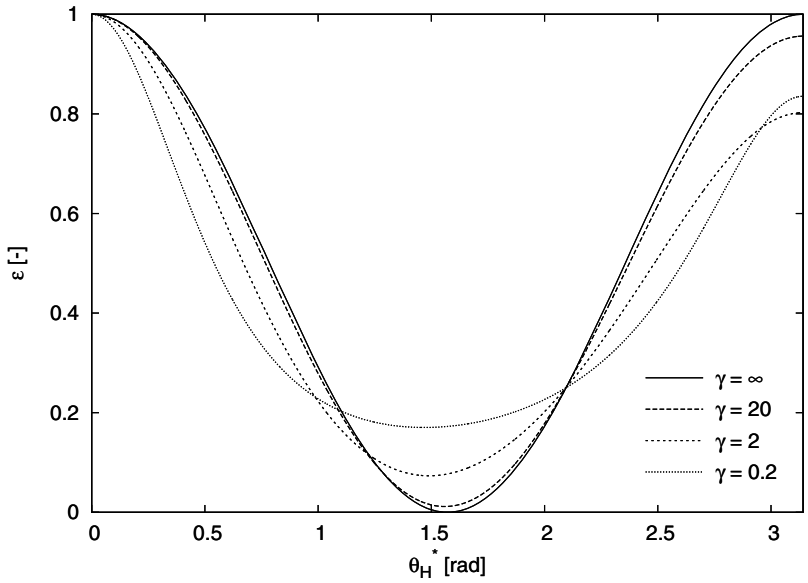

Figure 9: θ_H^* versus ε for four values of γ

4.5 Analysis of gait efficiency

In biped walking systems, unlike in rimless wheels, maximizing K^- is not always equivalent to maximizing the gait efficiency for the following reasons.

- The convergent level of K^- is not always equivalent to that of the walking speed.
- Even if the convergent kinetic energy is at a maximum, energy efficiency is not always maximum because it is evaluated in another way.

In this paper, we also consider an accurate control without PD feedback to examine the rigorous property of the desired-time trajectory. The initial conditions must be identical to the desired values in this case. If we apply the Jacobian matrix of Eq. (38) for transition, however, the angular velocity of relative hip-joint, $\dot{\theta}_H^+$, does not become zero. We therefore add another condition:

$$\dot{\theta}_H^+ = 0, \tag{62}$$

which represents the mechanical lock of the hip joint at impact. The Jacobian matrix of Eq. (38) then becomes

$$\hat{\boldsymbol{J}}_I(\alpha) = \begin{bmatrix} 1 & 0 & l\cos\theta_1 & -1 & 0 & -l\cos\theta_2 \\ 0 & 1 & -l\sin\theta_1 & 0 & -1 & l\sin\theta_2 \\ 0 & 0 & 0 & 1 & 0 & 0 \\ 0 & 0 & 0 & 0 & 1 & 0 \\ 0 & 0 & 1 & 0 & 0 & -1 \end{bmatrix}. \tag{63}$$

The Lagrange's undetermined multiplier vector of Eq. (32) and the angular velocity just after impact of Eq. (40) are calculated in the same manner by replacing $\boldsymbol{J}_I(\alpha)$ with $\hat{\boldsymbol{J}}_I(\alpha)$. The control input for

the tracking control is given only by the feed forward of angular acceleration. The vector $\boldsymbol{\Gamma}$ of Eq. (53) is thus determined as

$$\boldsymbol{\Gamma} = \begin{bmatrix} Mg\tan\phi\dot{X}_g \\ \ddot{\theta}_{H\mathrm{d}} + \boldsymbol{S}_2^{\mathrm{T}}\boldsymbol{M}(\boldsymbol{\theta})^{-1}\boldsymbol{h}(\boldsymbol{\theta},\dot{\boldsymbol{\theta}}) \end{bmatrix}. \tag{64}$$

By applying this approach, the tracking error can be completely zero. The difference between with and without PD feedback is discussed later.

4.5.1 When α is constant

Fig. 10 shows the analysis results of the constrained compass-gait when α is constant. All system parameters except α_1 and α_2 were chosen as the same values of Fig. 8. All indicated data are mean values. $\Delta\alpha := \alpha_1 - \alpha = \alpha - \alpha_2 \geq 0$ is used for the horizontal axis. Here, (a) is the walking speed, (b) the kinetic energy just before impact, (c) the energy-loss coefficient, (d) the restored mechanical energy, (e) the specific resistance, and (f) the step period. We can see that the larger $\Delta\alpha$ is, the more asymmetric the gait becomes. The value at which $\Delta\alpha = 0$ (1-period gait, symmetric) is plotted with a solid circle to distinguish it from other 2-period cases.

From Fig. 10 (a) and (b), we can see that the walking speed and kinetic energy monotonically decrease as the gait asymmetry grows. From (c) and (d), we can confirm that the two magnitude relations of Eqs. (12) and (14) hold. (e) and (f) are plotted for reference, and these results are explained as follows. Let ΔX_g [m] be the step length, and this is given by

$$\Delta X_g = l\left(\sin\alpha_1 + \sin\alpha_2\right) = 2l\sin\alpha\cos(\alpha - \alpha_1). \tag{65}$$

This is a constant, and its partial derivative with respect to α_1 becomes

$$\frac{\partial \Delta X_g}{\partial \alpha_1} = 2l\sin\alpha\sin(\alpha - \alpha_1) \leq 0. \tag{66}$$

Note that $\alpha_1 \geq \alpha$ holds. Therefore, the step length decreases as the gait becomes more asymmetrized when α is constant. The change ratio is, however, much smaller than that of the walking speed, and the step period then increases inversely with the decrease of walking speed. On the other hand, the minimum specific resistance in VPDW is $\tan\phi$ [-], and the specific resistance (SR) is kept $\tan\phi$ [-] if the maximum efficiency condition is achieved. There is a tendency, however, that the negative input power increases as the gait becomes more asymmetrized, and this caused the decrease in energy efficiency. See APPENDIX for further detailed discussions.

From Fig. 10(a), we can also see that the walking speed in the case without PD feedback is slower than that with PD feedback. We discuss the reason in the following. Kinetic energies just after and just before impact are respectively given by

$$K^+ = \frac{1}{2}\boldsymbol{\xi}(\alpha)^{\mathrm{T}}\boldsymbol{M}(\alpha)\boldsymbol{\xi}(\alpha)\left(\dot{\theta}_1^-\right)^2, \quad K^- = \frac{1}{2}\begin{bmatrix} 1 \\ 1 \end{bmatrix}^{\mathrm{T}}\boldsymbol{M}(\alpha)\begin{bmatrix} 1 \\ 1 \end{bmatrix}\left(\dot{\theta}_1^-\right)^2, \tag{67}$$

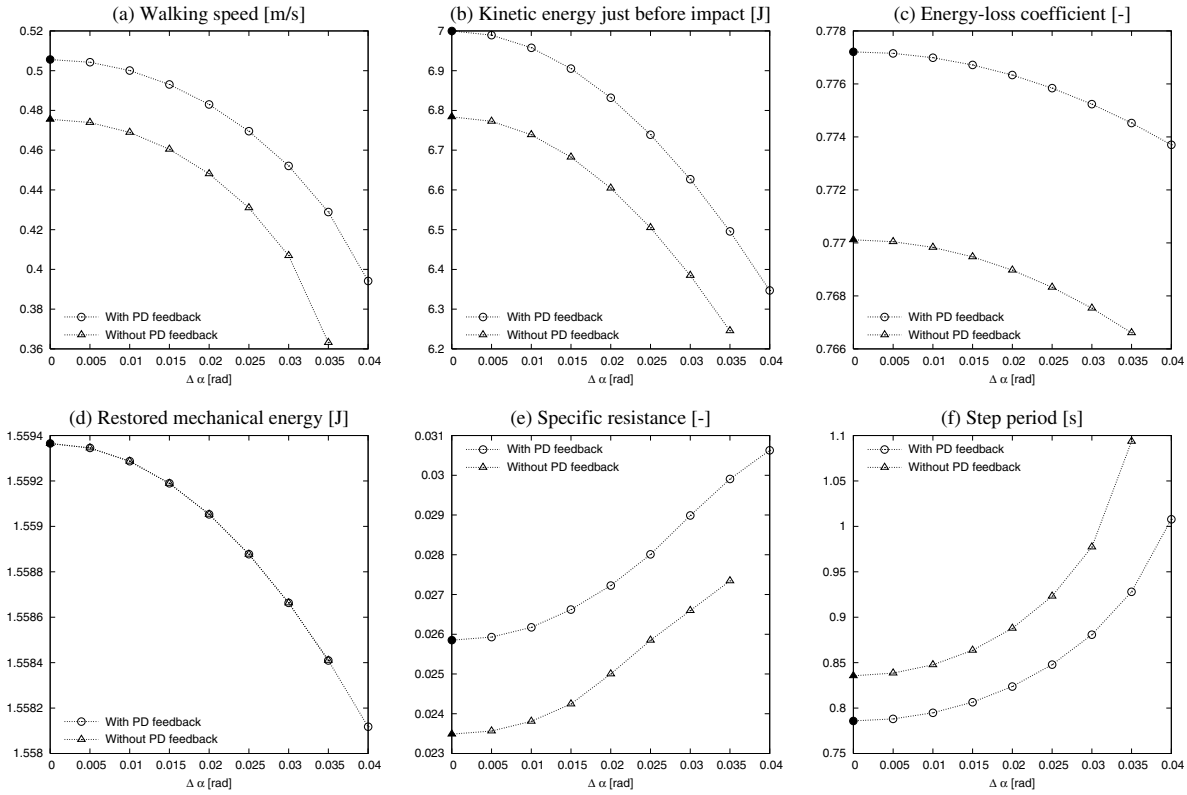

Figure 10: Gait descriptors of constrained compass-gait where α is constant

and the energy-loss coefficient is then defined as

$$\varepsilon = \frac{\boldsymbol{\xi}(\alpha)^{\mathrm{T}} \boldsymbol{M}(\alpha) \boldsymbol{\xi}(\alpha)}{\begin{bmatrix} 1 \\ 1 \end{bmatrix}^{\mathrm{T}} \boldsymbol{M}(\alpha) \begin{bmatrix} 1 \\ 1 \end{bmatrix}}. \tag{68}$$

Energy-loss coefficients in the cases with and without PD feedback are respectively calculated in the same manner above by using $\boldsymbol{J}_I(\alpha)$ or $\hat{\boldsymbol{J}}_I(\alpha)$. In this case, ε is also a function only of α and Fig. 11 plots the values in the two cases with respect to α. We can see that the value of ε without PD feedback is smaller than that with PD feedback. This is caused by adding one more constraint condition for achieving $\dot{\theta}_H^+ = 0$. In VPDW, however, the restored mechanical energies in both cases are the same if the step lengths are identical, and this is strongly supported by Fig. 10 (d). The kinetic energy just before impact, $K^- = \Delta E/(1-\varepsilon)$, then decreases as ε decreases. Therefore, we can conclude that the walking speed in the case without PD feedback accordingly decreased with respect to the decreases of ε and K^-. A small decrement of kinetic energy causes a significant decrement of walking speed.

4.5.2 When α_1 is constant

Fig. 12 shows the analysis results where α_1 is constant. The horizontal axis is the mean value of the hip-joint angle, α, except in (f) where α_1 and α_2 are used for the horizontal axis and we have indicated the corresponding step periods. From (a) and (b), we can see that the walking speed and

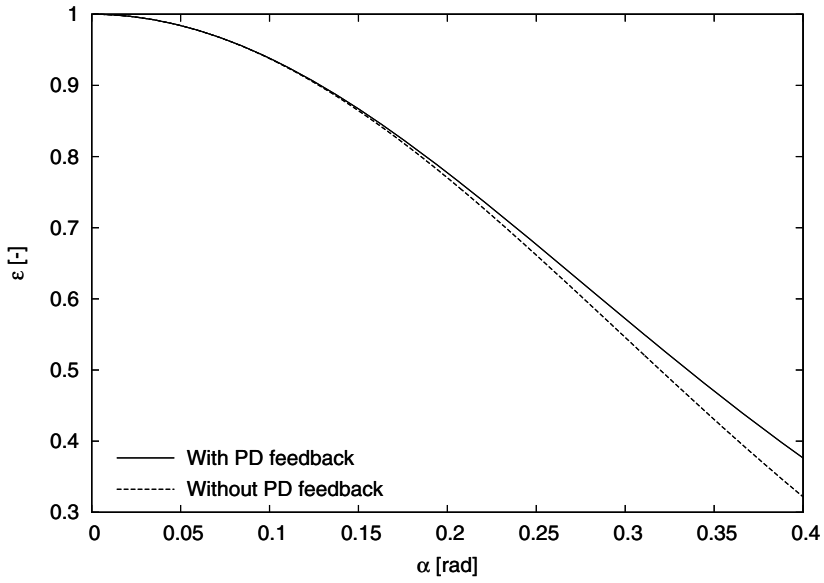

Figure 11: α versus ε in cases with and without PD feedback

kinetic energy increase with decreasing α. In contrast to the above case, the gait efficiency improves as the gait asymmetry grows. This means that the point on the line of $\alpha_1 = \alpha_2$ in Fig. 4 moves toward the left in the direction B. In contrast, if the point moves toward the right in the direction B, as Fig. 12 (b) indicates, the kinetic energy decreases. (c) shows that ε_m monotonically increases with decreasing α, i.e. with the mean value of the step length, in accordance with the constraint on the impact posture. Following Eqs. (57) and (65), it is shown that the following equality

$$\Delta E_m = Mg \tan\phi \Delta X_g \tag{69}$$

holds in a 2-period gait. This shows that ΔE_m monotonically decreases with decreasing α, and Fig. 12 (d) strongly supports it. (e) shows that the specific resistance grows worse as the gait becomes more asymmetrized. This result comes from the same reason previously described. See APPENDIX for further detail. We plotted the step period in (f) to show that the stable gait generation becomes impossible because the step period becomes too short to satisfy the settling-time condition. We can see that the step periods in both cases approach the desired settling-time, $T_{\rm set} = 0.75$ [s].

5 Conclusion and Future Work

We discussed the efficiency and optimality of a 2-period gait from the kinetic energy view-point. Numerical simulations of VPDW proved the validity of the method derived from the discrete dynamics of a rimless wheel. We must note, however, that a dynamic bipedal gait achieving the two magnitude relations of Eqs. (12) and (14) is limited.

In the future, we should theoretically investigate the relation between the convergent kinetic energy level and walking speed in more detail. Although a one-to-one relation between walking speed and

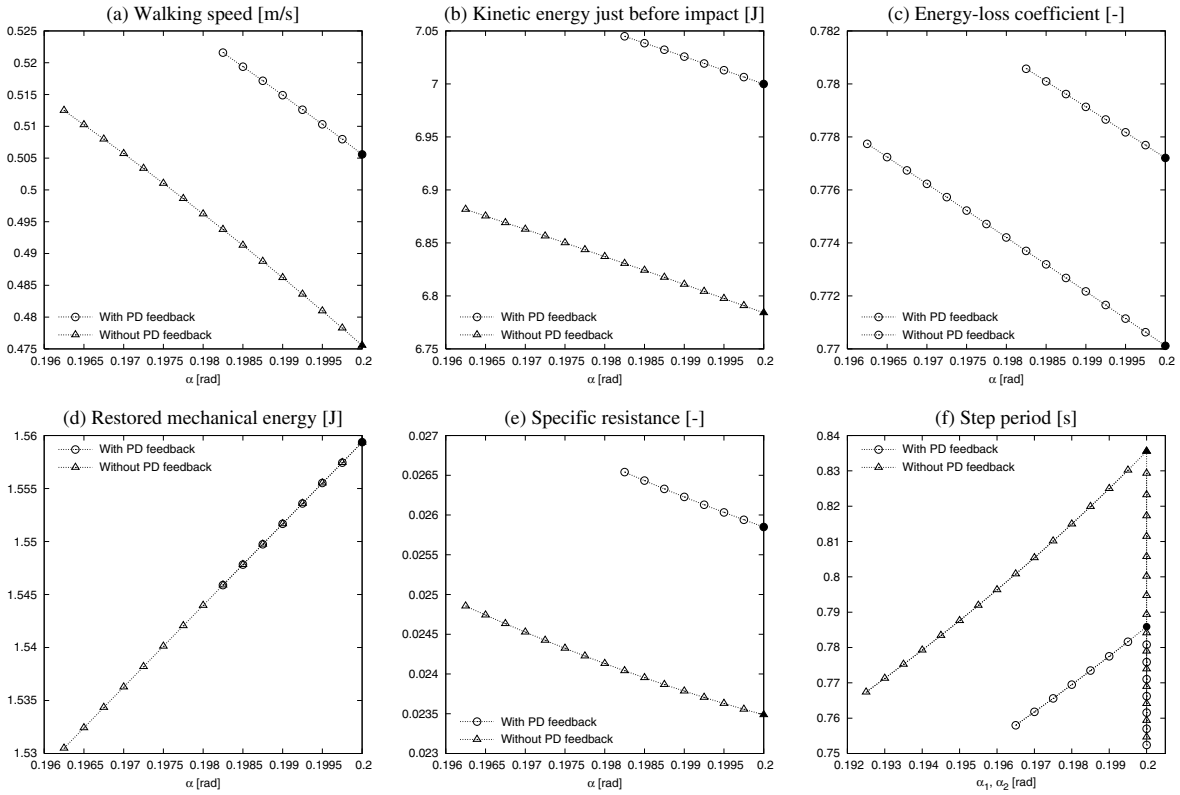

Figure 12: Gait descriptors of constrained compass-gait where α_1 is constant

kinetic energy holds for a rimless wheel, limit cycle walkers have leg-swing motions that destroys the one-to-one relation. The author considers that the swing-leg retraction is the cause [19]. On the other hand, the effects of hip damper and DFC as means of gait symmetrization on gait efficiency would also be an interesting subject. Extension of our approach to general multiple-period cases, i.e., 2^n-period and chaotic gaits, should also be investigated.

REFERENCES

[1] T. McGeer: "Passive dynamic walking," *Int. J. of Robotics Research*, Vol. 9, No. 2, pp. 62–82, April 1990.

[2] F. Asano, Z.-W. Luo and M. Yamakita: "Biped gait generation and control based on a unified property of passive dynamic walking," *IEEE Trans. on Robotics*, Vol. 21, No. 4, pp. 754–762, Oct. 2005.

[3] F. Asano and Z.-W. Luo: "Energy-efficient and high-speed dynamic biped locomotion based on principle of parametric excitation," *IEEE Trans. on Robotics*, Vol. 24, No. 6, pp. 754–762, Dec. 2008.

[4] A. Goswami, B. Thuilot and B. Espiau: "Compass-like biped robot part I: Stability and bifurcation of passive gaits," *Research report, INRIA*, No. 2996, 1996.

[5] M. Garcia, A. Chatterjee and A. Ruina: "Speed, efficiency, and stability of small-slope 2D passive dynamic bipedal walking," *Proc. of the IEEE Int. Conf. on Robotics and Automation*, Vol. 3, pp. 2351–2356, May 1998.

[6] M. Garcia, A. Chatterjee, A. Ruina and M. Coleman: "The simplest walking model: Stability, complexity, and scaling," *ASME J. of Biomechanical Engineering*, Vol. 120, No. 2, pp. 281–288, April 1998.

[7] M. Garcia, A. Chatterjee and A. Ruina: "Efficiency, speed, and scaling of two-dimensional passive-dynamic walking," *Dynamics and Stability of Systems*, Vol. 15, No. 2, pp. 75–99, June 2000.

[8] A. Goswami, B. Thuilot and B. Espiau: "A study of the passive gait of a compass-like biped robot: Symmetry and chaos," *Int. J. of Robotics Research*, Vol. 17, No. 12, pp. 1282–1301, Dec. 1998.

[9] A. Sano, Y. Ikemata and H. Fujimoto: "Analysis of dynamics of passive walking from storage energy and supply rate," *Proc. of the IEEE Int. Conf. on Robotics and Automation*, Vol. 2, pp. 2478–2483, Sep. 2003.

[10] K. Osuka and Kirihara, "Motion analysis and experiments of passive walking robot Quartet II," *Proc. of the IEEE Int. Conf. on Robotics and Automation*, Vol. 3, pp. 3052–3056, April 2000.

[11] E. Ott, C. Grebogi and J. A. Yorke, "Controlling chaos," *Physical Review Letters*, Vol. 64, No. 11, pp. 1196–1199, March 1990.

[12] K. Pyragas, "Continuous control of chaos by self-controlling feedback," *Physics Letters A*, Vol. 170, No. 6, pp. 421–428, Nov. 1992.

[13] Y. Sugimoto and K. Osuka, "Walking control of quasi passive dynamic walking robot "Quartet III" based on continuous delayed feedback control," *Proc. of the IEEE Int. Conf. on Robotics and Biomimetics*, pp. 606–611, Aug. 2004.

[14] S. Suzuki and K. Furuta: "Enhancement of stabilization for passive walking by chaos control approach," *Proc. of the 15th IFAC World Congress*, July 2002.

[15] F. Asano and Z.W. Luo: "Pseudo virtual passive dynamic walking and effect of upper body as counterweight," *Proc. of the IEEE/RSJ Int. Conf. on Intelligent Robots and Systems*, pp. 2934–2939, Sep. 2008.

[16] A. Ruina, J. E.A Bertram and M. Srinivasan, "A collisional model of the energetic cost of support work qualitatively explains leg sequencing in walking and galloping, pseudo-elastic leg behavior in running and the walk-to-run transition," *J. of Theoretical Biology*, Vol. 237, No. 2, pp. 170–192, Nov. 2005.

[17] K. Byl and R. Tedrake, "Metastable walking on stochastically rough terrain," *Proc. of the Robotics: Science and Systems IV*, June 2008.

[18] F. Asano and Z.-W. Luo, "Asymptotically stable biped gait generation based on stability principle of rimless wheel," *Robotica*, Vol. 27, No. 6, pp. 949–958, Oct. 2009.

[19] F. Asano, "Effects of swing-leg retraction and mass distribution on energy-loss coefficient in limit cycle walking," *Proc. of the IEEE/RSJ Int. Conf. on Intelligent Robots and Systems*, pp. 3214–3219, Oct. 2009.

APPENDIX

This appendix discusses the reason why the energy efficiencies in Figs. 10 and 12 worsened as the gait became more asymmetrized in more detail.

Let p_j [J/s] and v_j [m/s] be the average input power and the walking speed in the generated 2-period bipedal gait in section 4, and they are respectively given by

$$p_j := \frac{1}{T_j}\int_{0^+}^{T_j^-} \left(\left|\dot{\theta}_1 u_1\right| + \left|\dot{\theta}_H u_2\right|\right) \mathrm{d}t, \tag{70}$$

$$v_j := \frac{1}{T_j}\int_{0^+}^{T_j^-} \dot{X}_g \ \mathrm{d}t = \frac{\Delta X_g}{T_j}. \tag{71}$$

The subscript j (= 1 or 2) corresponds to that of ΔE_j in Eqs. (55) and (56). ΔX_g [m] is the step length given by (65), and this does not change in 2-period gait.

Using the above quantities, the specific resistance (SR) is defined as

$$\mathrm{SR} := \frac{p_j}{Mgv_j} = \frac{p_j T_j}{Mg\Delta X_g}, \tag{72}$$

which means the expenditure of energy per unit mass and per unit length, and this is a dimensionless quantity. The main question of how to attain energy-efficient biped locomotion rests on how to increase walking speed, v, while keeping p small. The smaller SR is, the better energy-efficiency is.

In VPDW, the average input power in Eq. (70) satisfies the following inequality.

$$p_j \geq \frac{1}{T_j}\int_{0^+}^{T_j^-} \left|\dot{\theta}_1 u_1 + \dot{\theta}_H u_2\right| \mathrm{d}t = \frac{1}{T_j}\int_{0^+}^{T_j^-} \left|\dot{E}\right| \mathrm{d}t \geq \frac{1}{T_j}\int_{0^+}^{T_j^-} \dot{E} \ \mathrm{d}t = \frac{Mg\tan\phi\Delta X_g}{T_j} \tag{73}$$

Therefore, the minimum SR in 2-period gait also becomes

$$\mathrm{SR} \geq \tan\phi. \tag{74}$$

Fig. 13 plots (a) the step length and (b) the consumed energy (the mean value of $p_j T_j$ [J]) in Fig. 6 with respect to $\Delta\alpha$. As Eqs. (65) and (66) indicate, from Fig. 6 (a) we can see that the step length monotonically decreases as the gait becomes more asymmetrized. If the maximum efficiency condition is achieved or negative input power does not occur, the following equality

$$p_j T_j = Mg\tan\phi\Delta X_g \tag{75}$$

holds. Therefore, the consumed energy must monotonically decrease as $\Delta\alpha$ decreases if the maximum efficiency condition is achieved. On the contrary, however, Fig. 13 (b) shows that the consumed energy increases as $\Delta\alpha$ increases. Therefore, we can conclude that the increase of SR comes from the negative input power.

Fig. 14 plots (a) the step length and (b) the consumed energy in Fig. 7 with respect to α. In this case, only α_2 monotonically decreases and it is thus obvious that the step length monotonically decreases with it. Therefore, the consumed energy must decrease as α_2 decreases if Eq. (75) holds or the maximum efficiency condition is achieved. Whereas from (b), we can see that the consumed energy monotonically increases as the gait becomes more asymmetrized. Therefore, we can conclude that the increase of SR comes from the same reason as the above case.

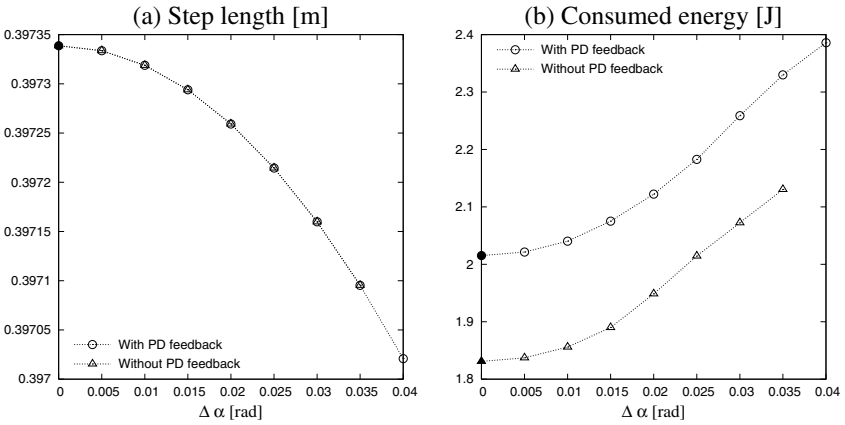

Figure 13: Step length and consumed energy with respect to $\Delta\alpha$ where α is constant

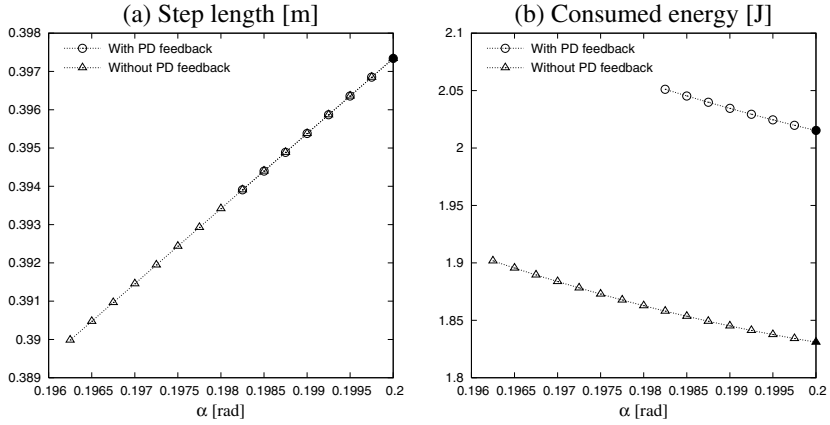

Figure 14: Step length and consumed energy with respect to α where α_1 is constant